

Supplementary Information:

Excited state dynamics and time-resolved photoelectron spectroscopy of *para*-xylylene

Kevin Issler,[†] Anja Röder,^{†,‡} Florian Hirsch,[†] Lionel Poisson,^{*,¶} Ingo Fischer,^{*,†}
Roland Mitrić,^{*,†} and Jens Petersen^{*,†}

[†]*Julius-Maximilians-Universität Würzburg, Institut für physikalische und theoretische
Chemie, Emil-Fischer-Str. 42, 97074 Würzburg, Germany*

[‡]*Present Address: Department of Chemistry, University of Ottawa, 10 Marie Curie,
Ottawa, Ontario K1N 6N5, Canada*

[¶]*LIDYL, CEA, CNRS, Université Paris-Saclay, CEA Saclay, 91191 Gif-sur-Yvette, France*

E-mail: lionel.poisson@cea.fr; ingo.fischer@uni-wuerzburg.de; roland.mitric@uni-wuerzburg.de;
jens.petersen@uni-wuerzburg.de

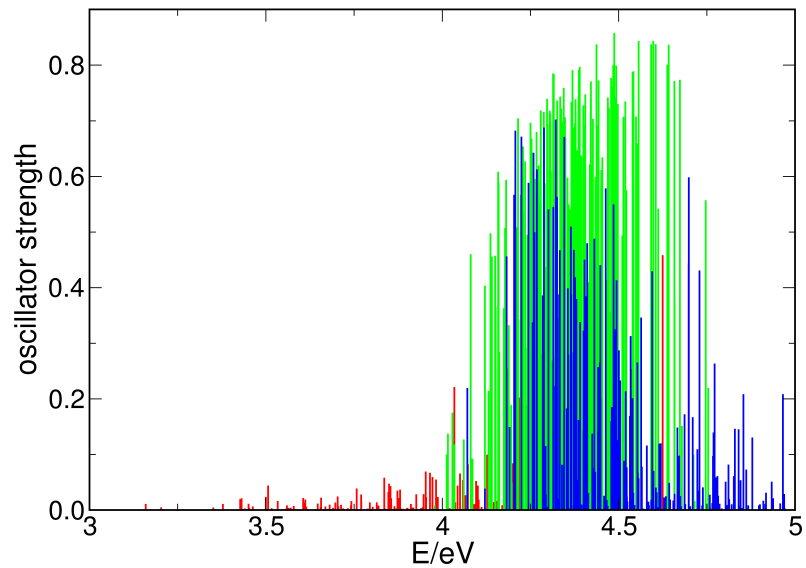


Fig. S1: Unconvolved absorption spectrum of the ensemble of trajectories. The sticks correspond to excitations from the ground state to the S_1 (red), S_2 (green) or S_3 states (blue).

Structures at Conical Intersections

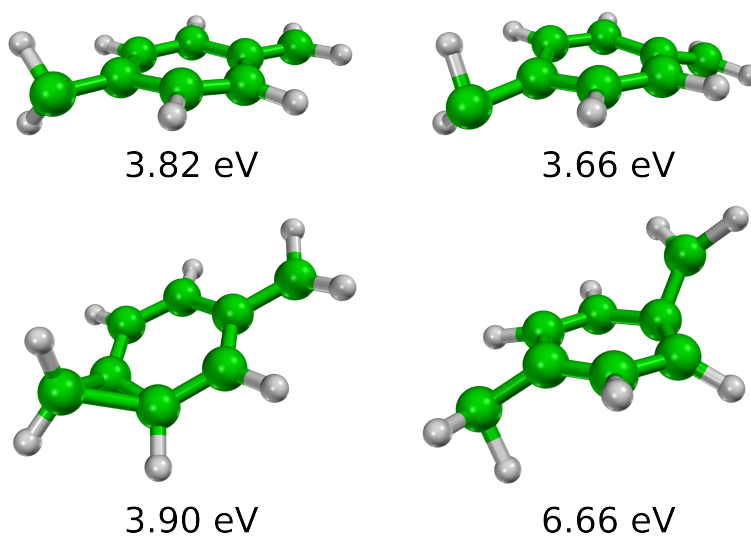


Fig. S2: Exemplary optimised molecular geometries at S_0 - S_1 -CIs relevant in the FISH dynamics and corresponding energies relative to the absolute ground state energy at the equilibrium geometry.

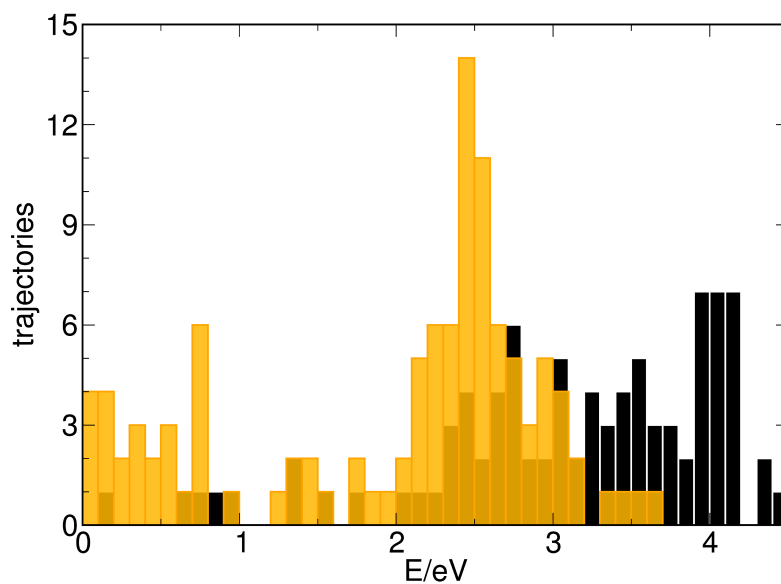


Fig. S3: Histogram of the S_1 - S_0 energy gaps of each trajectory at the last hop to the ground state; black: hops within the first 325 fs (laser pulse on), orange: hops after 325 fs (laser pulse off).

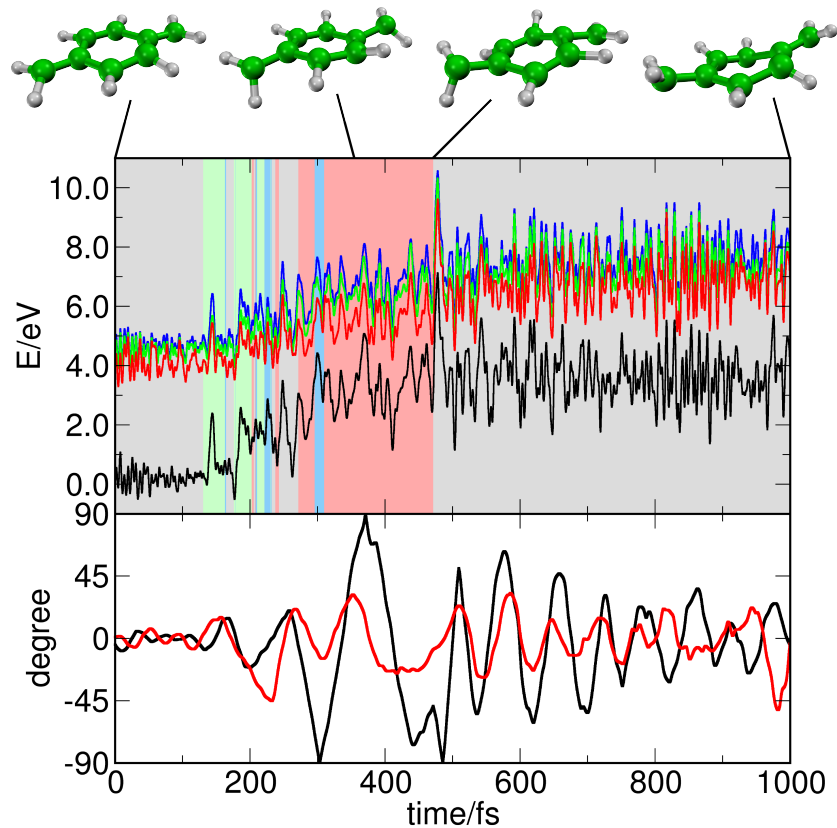


Fig. S4: Trajectory exhibiting the final hop to S_0 at an energy gap of ~ 2.5 eV (as shown in Fig. S3); upper part: state energies of the ground and lowest three excited states as well as molecular geometries at selected times (the lighter colours in the background indicate the occupied state); b) angle between the two pairs of methylene hydrogens and the average phenyl plane.

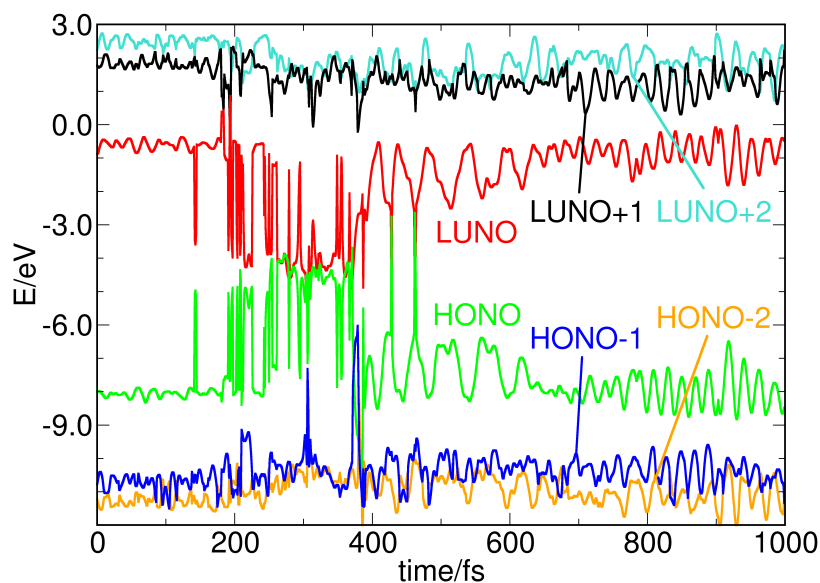


Fig. S5: Expectation values of the Fock operator (orbital energies) for the natural orbitals exhibiting the strongest deviations of their occupation numbers from zero or two, as shown in Fig. 5. The respective next higher and next lower energies (LUNO+2/HONO-2) are shown as well.

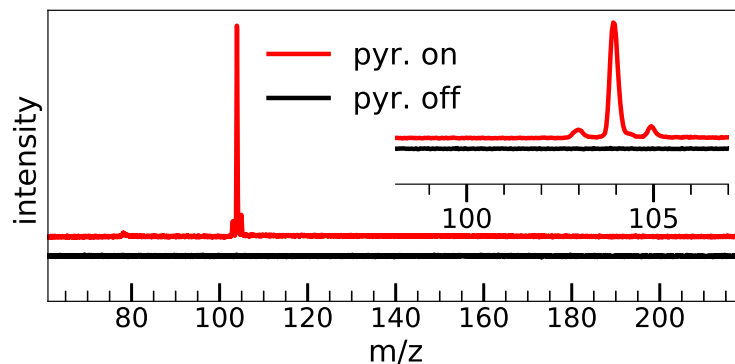


Fig. S6: Mass spectra with pyrolysis on and pyrolysis off at pump-probe conditions for 266 nm pump/794 nm probe wavelength.

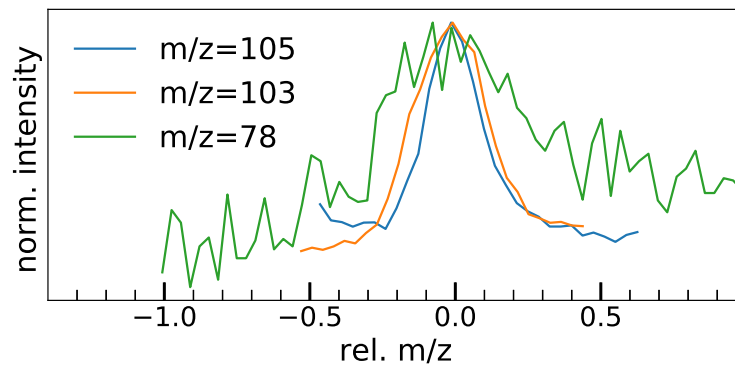


Fig. S7: Comparison of the peak shape for $m/z = 105$, 103 and 78 for $266\text{ nm}/794\text{ nm}$ at pump-probe conditions.

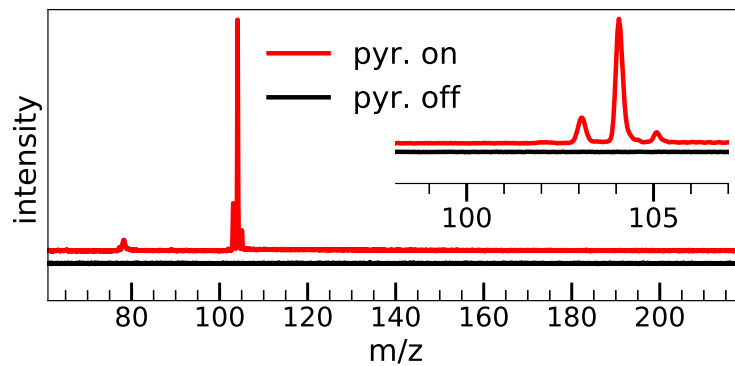


Fig. S8: Mass spectra with pyrolysis on and pyrolysis off at pump-probe conditions for 266 nm pump/ 397 nm probe wavelength.

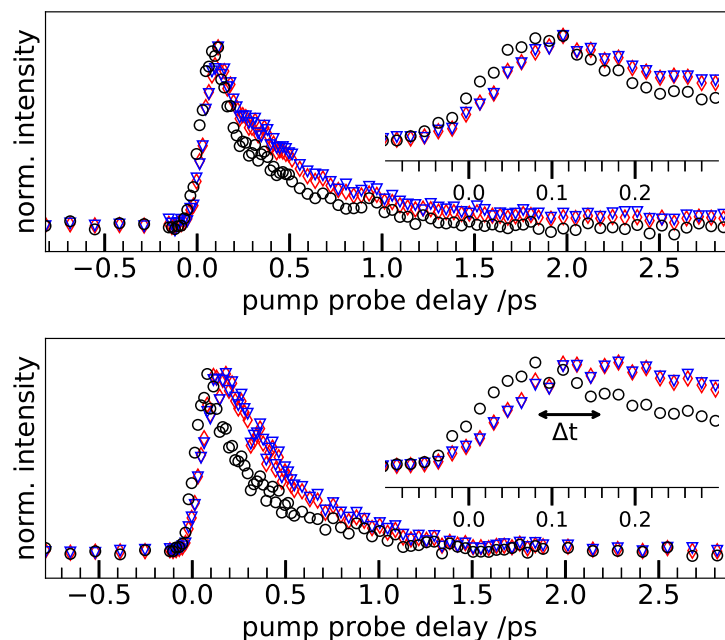


Fig. S9: Upper: Normalised decays of signals in the mass spectra at 397 nm probe wavelength. Experimental data of $m/z = 104$ (*para*-xylylene, black circles), 103 (red diamonds) and 78 (blue triangles). The time shift between $m/z = 78$ & 103 vs. 104 is not as clearly visible as with 794 nm probe (lower). Ionisation at 397 nm requires 2 photons, which is equivalent to the $[1+4']$ process with the 794 nm probe. An equivalent to the 3-photon process with 794 nm $[1+3']$ is not possible with 397 nm probe and fragmentation appears from the beginning of the dynamics.

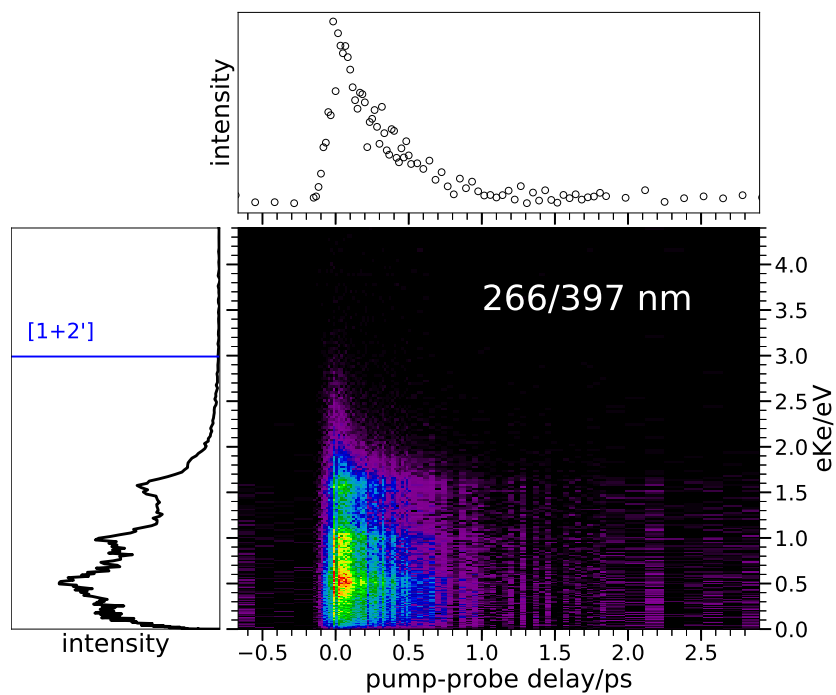


Fig. S10: TRPES with 266 nm pump/397 nm probe. The time dependence of the total photoelectron signal (top trace) can be fitted with a single time constant $\tau = 328$ fs. The graph on the left shows the photoelectron kinetic energy summed over all delay times.